FEDSM-ICNMM2010-'%0-(

EVALUATION OF TURBULENCE MODELS USING LARGE-EDDY SIMULATION DATA

Hassan Raiesi, Ugo Piomelli,*Andrew Pollard
Department of Mechanical and Material Engineering
Queen's University, Kingston (ON), Canada

ABSTRACT

The performance of some of the most commonly used eddy viscosity turbulence models to predict separated boundary layer flows in adverse pressure gradient has been evaluated against large eddy simulations. The LES results were used to assess the consistency of the different terms in the $k-\varepsilon$, $\zeta-f$, $k-\omega$ and Spalart-Allmaras models. For the separated boundary layer, the eddy-viscosity assumption works well, and anisotropic effects are not significant. However, the near-wall treatment used in $k-\varepsilon$ models was found to have a critical effect on the predictive accuracy of the flow (and, in particular, of separation and reattachment points). None of the wall treatments tested resulted in accurate prediction of the flow field.

1 Introduction

Turbulence models for the Reynolds averaged Navier-Stokes (RANS) equations have been widely utilized to calculate many scientific and engineering problems due to their reduced computational cost compared to the Direct Numerical and Large Eddy simulations (DNS, LES) [1]. DNS an LES can provide invaluable information about the details of the flow field, but their computational cost has limited their use to rather simple flows and geometries. Hence, the RANS approach will continue to be used in the foreseeable future specially in industrial environments.

The simplest class of turbulence models uses an eddy viscosity assumption to relate the Reynolds stresses to the mean strain rate tensor (Boussinesq assumption). Despite their popularity, there are many limitations and issues with the eddy viscosity models

mentioned in the literature [2], [3], which are however largely unquantified. The principal feature of these models is the assumption of isotropic eddy viscosity in the calculation of turbulence stresses. The low-Reynolds-number flow regions near no-slip walls, however display strong anisotropy both in the boundary layer and in the separated recirculating zone, which cannot be accurately captured by any linear eddy viscosity model. The poor performance of RANS models near solid boundaries may cause erroneous predictions of the flow in the outer region [4, 5]. Other known issues with these models include response to perturbations, effects of streamline curvature, return to equilibrium and system rotation.

Testing of RANS models is usually performed through the calculation of standard canonical cases: among them are flat plate boundary layer, flow over a backward facing step, accelerating boundary layer and massively separated flows (flow over a cylinder, etc) and comparison with experiments. The test case considered in the present study is mild boundary layer separation. We consider the turbulent flow over a flat plate with a suction and blowing velocity profile imposed in the freestream to induce a strong adverse pressure gradient that cause the flow to separate and then to reattach. In the current test case, flow separation is triggered by the adverse pressure gradient. This is unlike the backward facing step, where the flow separation forms due to an abrupt change in the geometry that fixes the point of separation. Therefore, the prediction of both separation and reattachment is a more challenging task, yet because of the simple geometry of the problem, numerical errors can be controlled.

The goal of this paper is to test some of the most commonly used RANS models to quantify errors. These errors include the modelling of particular terms in each model and the Boussinesq approximation itself in the calculation of a class of flows

---

*Corresponding author. Email: ugo@me.queensu.ca.

of aeronautical interest. To achieve this, a reference data set that provides detailed information about the flow field is required in order to calculate the exact values of terms in RANS models. This reference dataset must not be affected by modelling, measurements errors and approximations. Direct numerical simulation can provide this type of information, but DNS is currently limited to very low-Reynolds number flows while most RANS models are designed and calibrated for high Reynolds flows, although there are modifications that may be applied for the low-Reynolds number near-wall regions. Therefore, the reference dataset must be also generated at the range of Reynolds number where good performance of RANS models is expected. Here, we used a bootstrapping technique: the problem was first solved using DNS at a low Reynolds number, and the results obtained from LES were validated against this reference calculation. LES calculations were then performed at higher Reynolds numbers using the same grid resolution as the low-Re LES calculation. These LES data were time averaged and used *a priori* to evaluate the validity of the Boussinesq approximation and the near-wall treatment; these comparisons are not affected by modelling assumptions, since the LES data were used. The LES also supply data for comparisons in which some of the modelled terms in the RANS equations are substituted by their exact values and the model performance is then evaluated by solving the remaining differential equations. This testing methodology has been proposed by Parneix and Durbin [6] and applied to second moment closure modeling of the turbulent flow over a backward facing step. This technique is very helpful to isolate potential modeling errors due to a particular term in a highly coupled system of equations. Finally, the LES provides data for *a posteriori* comparisons in which the advantage is that the boundary conditions can be matched more closely.

There are several eddy-viscosity models proposed by the turbulence research community. Among these closure models, it is difficult to favor one over the other. Most of these models produce quite satisfactory results for the test cases against which they were calibrated; however, when applied to other problems, they are not always reliable. The models selected in this study are based on their ability to predict the standard back-step flow and their popularity. We report the results of tests of four RANS models; the low-Reynolds-number $k - \varepsilon$ model in the Yang and Shih [7] formulation, the RNG $k - \varepsilon$ model of Yakhot *et al.* [8,9], the $k - \omega$ model by Wilcox [10], the one equation model of Spalart-Allmaras [11] and the $\zeta - f$ model derived by Hanjalic [12] as a variant of Durbin's $v^2 - f$ [13] model applied to a boundary layer with separation.

2 Problem formulation

2.1 Governing equations and numerical method

The governing equations solved in this problem are either the filtered or the time-averaged conservation of mass and momentum for an incompressible flow:

$$\frac{\partial \overline{u}_j}{\partial x_j} = 0 \tag{1}$$

$$\frac{\partial \overline{u}_i}{\partial t} + \frac{\partial \overline{u}_j \overline{u}_i}{\partial x_j} = \nu \frac{\partial^2 \overline{u}_i}{\partial x_j \partial x_j} - \frac{1}{\rho} \frac{\partial \overline{p}}{\partial x_i} - \frac{\partial \tau_{ij}}{\partial x_j}. \tag{2}$$

Here, an overline denotes either a filtered or a time-averaged quantity, and τ_{ij} are either the subgrid-scale (SGS) stresses, $\overline{u_i u_j} - \overline{u}_i \overline{u}_j$ or the Reynolds stresses $\overline{u'_i u'_j}$. The governing equations were solved in either LES or DNS mode by the specification of an appropriate parametrization for τ_{ij}. In the LES the SGS stresses are modelled using the Lagrangian-Averaged Dynamic Eddy-Viscosity model (LDEV) [14]. The models employed in the RANS calculations will be described below.

Two codes were used: for the LES we employed a finite-difference code [15], based on a staggered grid. Second-order central differences are used for both convective and diffusive terms, and a semi-implicit time-advancement scheme is used: the Crank-Nicolson scheme is used for the wall normal diffusive term, while a low-storage 3rd-order Runge-Kutta method is applied to the remaining terms. The solution of the Poisson equation is obtained by means of a Fourier-transform of the equation in the spanwise direction, followed by a cosine transform of the resulting equation in x, and by direct solution of the resulting tri-diagonal matrix, at each wavenumber. Note that when transforming the equations in Fourier space the modified wavenumber corresponding to the consistent central scheme is used in place of the actual wavenumber. The code is parallelized using the MPI protocol. For the RANS computations, a second order finite volume code based on a pressure correction algorithm [16] was employed. Diffusive term was discretized using a second-order central-difference scheme. For the convective term, a second order finite difference scheme was implemented through a defered correction algorithm to avoid numerical dissipation.

2.2 Turbulence models

Based on our aim, which is to evaluate models in widespread use within the aerospace industry, we considered eddy-viscosity models for the Reynolds stresses:

$$\tau_{ij} = -2\nu_T (S_{ij} - \frac{1}{3}\delta_{ij}S_{kk}) + \frac{2}{3}k\delta_{ij} \tag{3}$$

2

where $k = \tau_{kk}/2$ is the turbulent kinetic energy (TKE).

2.2.1 Spalart-Allmaras model

The one equation model by Spalart-Allmaras [11] is widely used in aeronautical applications. In this model, the transport equation for the eddy viscosity is written as

$$\frac{D\tilde{v}}{Dt} = C_{b1}\tilde{S}\tilde{v} - c_{w1}f_w\left(\frac{\tilde{v}}{d}\right)^2 + \frac{1}{\sigma}\frac{\partial}{\partial x_k}\left[(v+\tilde{v})\frac{\partial \tilde{v}}{\partial x_k}\right]$$
$$+ \frac{c_{b2}}{\sigma}\frac{\partial \tilde{v}}{\partial x_k}\frac{\partial \tilde{v}}{\partial x_k} \tag{4}$$

where the closure coefficients and auxiliary functions are defined as

$$v_T = \tilde{v}f_{v1}$$
$$c_{b1} = 0.1355, \quad c_{b2} = 0.622, \quad c_{v1} = 7.1, \quad \sigma = \tfrac{2}{3}$$
$$c_{w1} = \frac{c_{b1}}{\kappa^2} + \frac{1+c_{b2}}{\sigma}, \quad c_{w2} = 0.3, \quad c_{w3} = 2, \quad \kappa = 0.41$$
$$f_{v1} = \frac{\chi^3}{\chi^3 + c_{v1}^3}, \quad f_{v2} = 1 - \frac{\chi}{1+\chi f_{v1}}$$
$$f_w = g\left[\frac{1+c_{w3}^6}{g^6+c_{w3}^6}\right]^{1/6},$$
$$\chi = \frac{\tilde{v}}{v}, \quad g = r + c_{w2}(r^6 - r), \quad r = \frac{\tilde{v}}{\tilde{S}\kappa^2 d^2}$$
$$S = \sqrt{2\Omega_{ij}\Omega_{ij}}, \quad \Omega_{ij} = \tfrac{1}{2}(\partial u_i/\partial x_j - \partial u_j/\partial x_i)$$
$$\tilde{S} = S + \frac{\tilde{v}}{k^2 d^2}f_{v2}$$

and d is the distance from the closest solid boundary. The additional transition correction terms are not included in this study.

2.2.2 $k - \varepsilon$ model

For the $k - \varepsilon$ model, the transport equations for the turbulent quantities are written as

$$\frac{Dk}{Dt} = \frac{\partial}{\partial x_j}\left[(v + \frac{v_T}{\sigma_k})\frac{\partial k}{\partial x_j}\right] + P_k - \varepsilon \tag{5}$$
$$\frac{D\varepsilon}{Dt} = \frac{\partial}{\partial x_j}\left[(v + \frac{v_T}{\sigma_\varepsilon})\frac{\partial \varepsilon}{\partial x_j}\right] + (C_{\varepsilon 1}P_k - C_{\varepsilon 2}\varepsilon + E)T^{-1}. \tag{6}$$

Here, $P_k = -\overline{u_i u_j}U_{i,j}$ is turbulent energy production and ε is the dissipation rate of the turbulent kinetic energy. In the above equations, U_i are the Cartesian mean velocity components, x_i are the corresponding coordinates and $\frac{D}{Dt}$ is the material derivative. The first $k - \varepsilon$ model adopted here is the low Reynolds number model of Yang and Shih [7] where the realizable time scale is defined as $T = \frac{k}{\varepsilon} + (\frac{v}{\varepsilon})^{\frac{1}{2}}$ with the following model constants:

$\sigma_k = 1.0, \sigma_\varepsilon = 1.3, C_{\varepsilon 1} = 1.44, C_{\varepsilon 2} = 1.92$. The extra dissipation rate and turbulent viscosity are defined as

$$E = v v_T \frac{\partial^2 U_i}{\partial x_j \partial x_k}\frac{\partial^2 U_i}{\partial x_j \partial x_k} \tag{7}$$
$$v_T = C_\mu f_\mu \frac{k^2}{\varepsilon} \tag{8}$$

The damping function, f_μ, is defined as a function of the turbulence Reynolds numbers, $Re_y = \frac{\sqrt{k}y_n}{v}$

$$f_\mu = [1 - \exp(-a_1 Re_y - a_3 Re_y^3 - a_5 Re_y^5)]^{\frac{1}{2}} \tag{9}$$

and $a_1 = 1.5e - 4, a_3 = 5.0e - 7, a_5 = 1.0e - 10$ and $C_\mu = 0.09$.

The second approach we used was a two-layer wall model of Chen and Patel [17] in which the $k-$equation is solved everywhere, but the $\varepsilon-$ equation is replaced with the following equation along with a simple relation for the eddy viscosity in near-wall regions:

$$\varepsilon = k^{\frac{3}{2}}/l_\varepsilon$$
$$l_\varepsilon = C_l y\left(1 - e^{-Re_y/A_\varepsilon}\right)$$
$$v_T = C_\mu \sqrt{k}l_v$$
$$l_v = C_l y\left(1 - e^{-Re_y/A_v}\right) \tag{10}$$

where $A_\varepsilon = 2C_l, C_l = \kappa/C_\mu^{\frac{3}{4}}$ and $\kappa = 0.41, \quad A_v = 65$.

The $k - \varepsilon$ model by Yakhot *et al.* [8, 9] was derived based on the Renormalization Group (RNG) method by systematically removing small scales of the flow and has shown superior performance in the calculation of turbulent separated flows [18]. The model equations are different from the above $k - \varepsilon$ model with the following modifications:

$$E = -\frac{\eta(\eta - \eta_0)}{1 + \beta \eta^3}P_k$$
$$T = \frac{k}{\varepsilon}$$
$$v_T = C_\mu \frac{k^2}{\varepsilon}$$
$$S = \sqrt{2S_{ij}S_{ij}}, \quad S_{ij} = \tfrac{1}{2}(\partial u_i/\partial x_j + \partial u_j/\partial x_i)$$
$$C_\mu = 0.085, \quad C_{\varepsilon 1} = 1.42, \quad C_{\varepsilon 2} = 1.68$$
$$\sigma_k = \sigma_\varepsilon = 0.718, \quad \beta = 0.015,$$
$$\eta_0 = 4.38, \quad \eta = Sk/\varepsilon \tag{11}$$

In this study, the RNG $k - \varepsilon$ model was also solved with the two-layer wall treatment in the calculation of the separated boundary layer.

2.2.3 $\zeta - f$ **model** The next eddy viscosity model, the $\zeta - f$ model of Hanjalic *et al.* [12] was employed. This model is a variant of the $v^2 - f$ model [13] and solves a transport equation for the velocity scale ratio $\zeta = v^2/k$ instead of v^2 and based on Durbin's elliptic relaxation concept to capture non-viscous wall effects but benefits from a less numerically stiff boundary condition. The model equations are

$$v_T = C_\mu \zeta k T \tag{12}$$

$$\frac{D\zeta}{Dt} = f - \frac{\zeta}{k} P_k + \frac{\partial}{\partial x_j}[(v + \frac{v_T}{\sigma_\zeta})\frac{\partial k}{\partial x_j}] \tag{13}$$

$$L^2 \nabla^2 f - f = \frac{1}{T}\left(c_1 + c_2' \frac{P_k}{\varepsilon}\right)(\zeta - \frac{2}{3}) \tag{14}$$

In the above equation, the realizable time and length scales [19] are defined as

$$T = \max\left[\min\left(\frac{k}{\varepsilon}, \frac{a}{\sqrt{6}C_\mu |S| \zeta}\right), C_\tau(\frac{v}{\varepsilon})^{1/2}\right] \tag{15}$$

$$L = C_L \max\left[\min\left(\frac{k^{3/2}}{\varepsilon}, \frac{k^{1/2}}{\sqrt{6}C_\mu |S| \zeta}\right), C_\eta(\frac{v^3}{\varepsilon})^{1/4}\right]$$

The model equations are solved along with the transport equations for the turbulent kinetic energy and its dissipation rate. The constants are:

$$E = 0 \tag{16}$$
$$C_{\varepsilon 1} = 1.4(1 + 0.012/\zeta), \quad C_\mu = 0.22$$
$$c_1 = 0.4, \quad c_2' = 0.65 \quad |S| = \sqrt{S_{ij}S_{ij}}$$
$$\sigma_k = 1.0, \quad \sigma_\varepsilon = 1.3, \quad \sigma_\zeta = 1.2$$
$$C_\tau = 6.0, \quad C_L = 0.36, \quad C_\eta = 85$$

where the following boundary condition is used for the relaxation parameter f and the dissipation rate ε at the no-slip boundary

$$f_w = \lim_{y \to 0} \frac{-2v\zeta}{y^2} \tag{17}$$

$$\varepsilon_w = \lim_{y \to 0} \frac{2vk}{y^2}$$
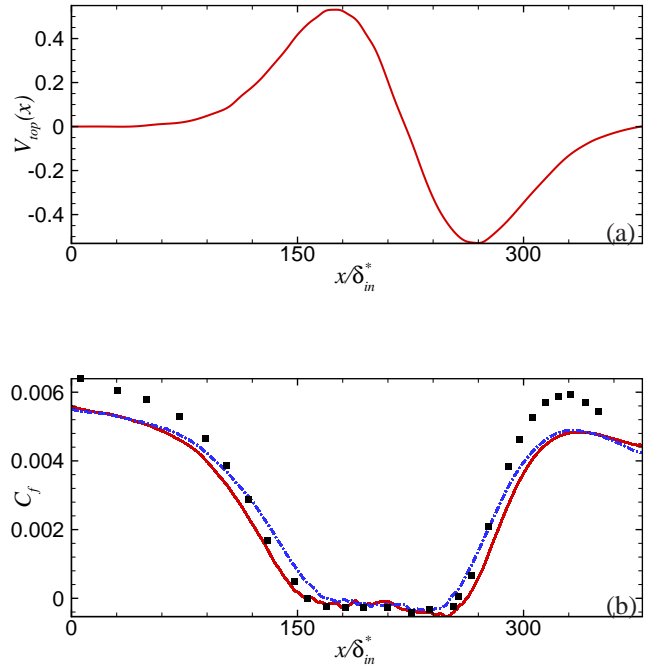
FIGURE 1. Boundary layer, $Re_{\delta_{in}^*} = 550$. (a) Vertical velocity profile along the top boundary. (b) Distribution of friction coefficient; □ : DNS [20], ——— : Present DNS, —··— : LES.

2.2.4 $k - \omega$ **model** For the $k - \omega$ model, the transport equations are

$$\frac{Dk}{Dt} = \frac{\partial}{\partial x_j}[(v + \frac{v_T}{\sigma_k})\frac{\partial k}{\partial x_j}] + P_k - \beta^* k\omega \tag{18}$$

$$\frac{D\omega}{Dt} = \frac{\partial}{\partial x_j}[(v + \frac{v_T}{\sigma_\omega})\frac{\partial \omega}{\partial x_j}] + \alpha\frac{\omega}{k}P_k - \beta\omega^2 \tag{19}$$

and the model constants are $\alpha = \frac{5}{9}, \beta = \frac{3}{40}, \beta^* = \frac{9}{100}, \sigma_k = \sigma_\varepsilon = 1.2$. The turbulent viscosity is then defined as

$$v_T = k/\omega. \tag{20}$$

The $k - \omega$ model equations can be integrated through the sublayer without introducing viscous modifications for turbulent boundary layers.

3 Boundary layer with separation

3.1 Validation of the LES

The test case considered here is the flow over a flat plate with a vertical velocity profile imposed at the top of the boundary to

4

induce a strong adverse pressure gradient that causes the flow to separate. DNS of this flow was first studied by Na and Moin [20]; we use the same configuration and parameters of their calculation, including the distribution of the vertical velocity, shown in Figure 1(a).

The computational domain is a Cartesian box of length $800 \times 96 \times 75$ in streamwise, wall normal and spanwise directions respectively. All dimensions are normalised by δ_o^*, the displacement thickness of the boundary layer at the reference location, $x = 0$. Direct numerical simulation of this problem at $Re_{\delta^*} = 550$ was first performed using $1024 \times 192 \times 192$ grid points; the resolution of $\Delta x^+ = 18$, $\Delta y_{min}^+ = 0.33$ and $\Delta z^+ = 11$ (the same as one of the cases in Ref. [20]). The LES code was used, with the SGS stresses set to zero. Recycling boundary conditions [21] are used to provide the velocity at the inlet, which is located $65\delta_o^*$ upstream of the reference location; in this region, the flow is a nominally zero-pressure-gradient (ZPG) boundary layer; for $x > 0$ the vertical velocity shown in Figure 1(a) is imposed at the freestream that creates an adverse pressure gradient (APG). The streamwise component of the velocity field at the top of the boundary is calculated by forcing the vorticity to be zero at the top boundary.

Next a large eddy simulation of the same problem was carried out to validate the LES model, and estimate the errors to be expected when coarser grids are used. The LES used $512 \times 192 \times 128$ grid points, giving $\Delta x^+ = 36$, $\Delta y_{min}^+ = 0.33$ and $\Delta z^+ = 22$. In Figure 1(b) the friction coefficient, $C_f = 2\tau_w/\rho U_o^2$ is shown (U_o is the freestream velocity at $x = 0$). Very good agreement with the reference data was obtained in the region of interest. There is a disagreement in the predicted C_f at the beginning of the domain, which is due to different techniques used in the generation of the inflow condition for the LES and DNS simulations. We used recycling, while Na and Moin [20] used a less realistic method based on assigning a frozen DNS field with randomization of the amplitude factors. More importantly, the difference between LES and DNS performed with the same code and boundary conditions is quite small: the maximum error in prediction of friction coefficient is 5%. Other quantities (mean velocity profiles and Reynolds stresses) also showed good agreement between the present DNS and LES and the reference data [20].

Turbulence models are designed for high-Reynolds-number flows; verification of their accuracy using this configuration would not give useful results; a higher Re is preferable for our goal. Thus, we carried out an LES at a higher Reynolds number, $Re_{\delta_o^*} = 2200$ on a domain of dimensions $800 \times 96 \times 75$. The grid uses $2560 \times 386 \times 386$ points, resulting in resolution (in wall units) similar to the low-Re LES: $\Delta x^+ = 31$, $\Delta y_{min}^+ = 0.56$ and $\Delta z^+ = 19$. The results obtained from this calculation were used for *a priori* and *posteriori* tests of the RANS models. Figure 2 shows the mean streamlines obtained from this calculation, and
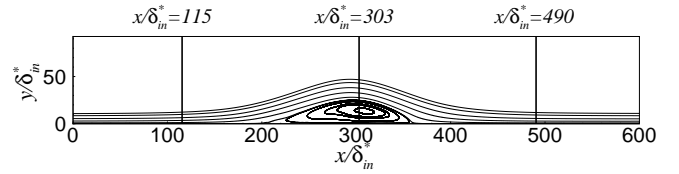
FIGURE 2. Mean streamlines, $Re_{\delta_o^*} = 2200$

three vertical lines where velocity profiles obtained from the LES will be compared with those from the RANS models.

3.2 *A priori* **tests of the turbulence models**

The LES data allows us to verify the accuracy of the RANS approach *a priori*, by using the LES data in the definition of the eddy viscosity, for instance. A first test examined the validity of the eddy-viscosity assumption. We define ν_T obtained using the LES data:

$$\nu_T = -\frac{\overline{u_i u_j}^{LES} S_{ij}^{LES}}{2 S_{ij}^{LES} S_{ij}^{LES}}. \tag{21}$$

where the "LES" superscript indicates a quantity obtained using the LES data. This value of ν_T is then used in the momentum equation (2); no transport equation for the turbulent quantities (k, ε, ω or $\tilde{\nu}$) is solved.

Since in this flow the shear stress is dominant in the transport of momentum, the eddy-viscosity assumption can be expected to work well. In fact, Figure 3 shows that the prediction of the friction coefficient and velocity profiles are in good agreement with the LES simulation. The separation and reattachment points are captured fairly accurately. Some errors are observed only in the separated flow region; in the attached boundary layer the eddy-viscosity assumption is accurate enough.

The second test we perform is one in which the values of k and ε from the LES are used in the definition of ν_T, Equations (8) and (20) respectively:

$$\nu_T = c_\mu f_\mu^{LES} \frac{(k^{LES})^2}{\varepsilon^{LES}}; \quad \nu_T = \frac{k^{LES}}{\omega}; \quad \nu_T = C_\mu \zeta k^{LES} T^{LES}. \tag{22}$$

For the $k - \varepsilon$ model, this implies that no transport equation is solved, while for the $k - \omega$ model, Equation (19) is solved, using k^{LES} in the production term. For the $\zeta - f$ model, only the transport equations for ζ and f were solved and $k^{LES}, \varepsilon^{LES}$ were used in the source terms and the definition of the eddy viscosity in equation (12).
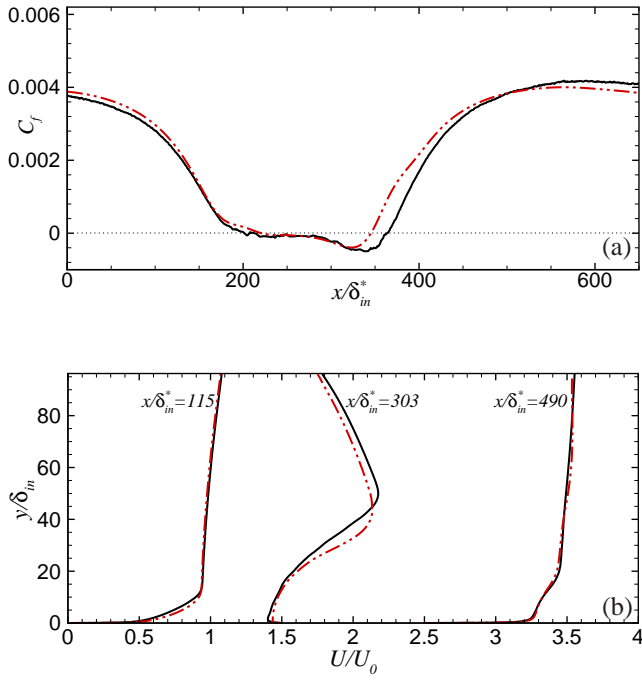
FIGURE 3. RANS prediction of friction coefficient and streamwise velocity profiles obtained from exact eddy viscosity (21); ——— LES, —··— RANS

The distribution of C_f obtained with this approach is compared to the LES data in Figure 4. We also show the friction coefficient obtained when the transport equations (5-6) or (18-19) are solved. For $k - \varepsilon$ and $k - \omega$ models we see that the agreement in the ZPG region is not very good (actually worse than if the transport equations are solved), but the results obtained from the $\zeta - f$ model shows consistent improvement up to the reattachment point once k^{LES} and ε^{LES} are used. The prediction of the recovery downstream of the separation bubble is also not accurate. The fact that both $k - \varepsilon$ and $k - \omega$ models are more accurate when transport equations are solved than if the "exact" values are supplied indicates, first, that the wall treatment plays an important role. Secondly, and perhaps more importantly, that error cancellation also has an important effect. It is well-known that in channel calculations, the $k - \omega$ model under-predicts k in the near-wall region [22], but gives the correct eddy viscosity distribution.

The relatively poor performance of the low-Re number $k - \varepsilon$ model, suggest that the definition of eddy viscosity itself (8) is not accurate in this test case; a different definition of f_μ would be required to improve the flow prediction. The exact value of
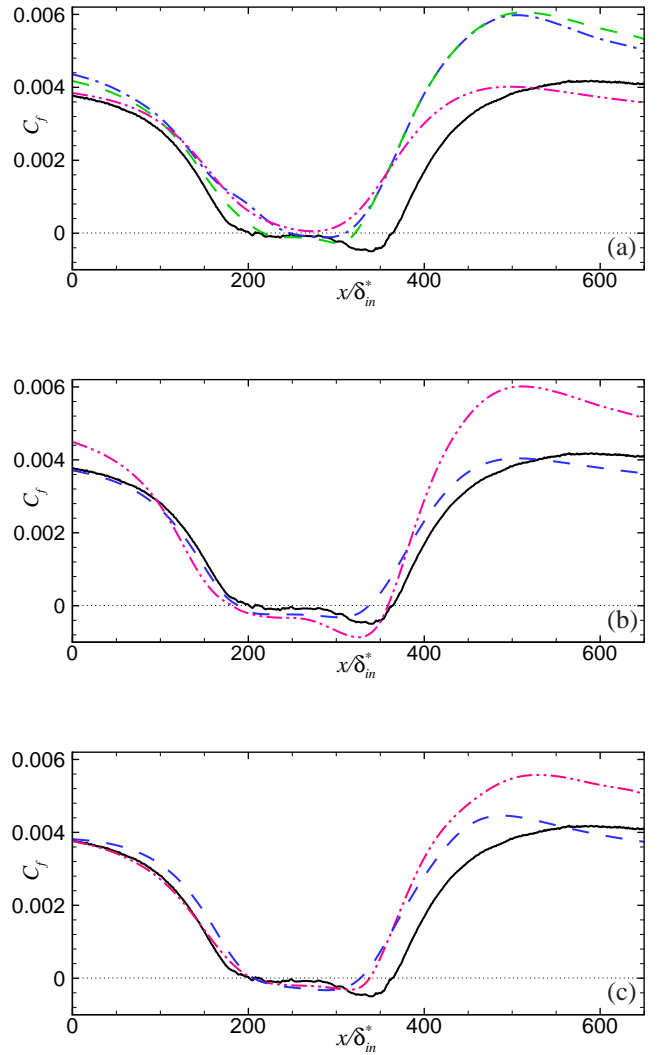
FIGURE 4. Distribution of friction coefficient. (a) $k - \varepsilon$ model; ——— LES; —·— ν_T from (22); --- Two-layer wall treatment; —··— Low-Re model. (b) $k - \omega$ model; ——— LES; --- ν_T from (20); —··— ν_T from (22) (c): $\zeta - f$ model; ——— LES; --- model prediction; —··— model prediction with exact k and ε

f_μ is calculated and plotted in Figure 5.

$$f_\mu^{LES} = \left[\frac{\overline{u_i u_j} \varepsilon}{2 S_{ij} c_\mu k^2} \right]^{LES} \tag{23}$$

Although there are many different forms of f_μ available for various low-Reynolds number eddy viscosity models, all of them are designed to provide the necessary level of damping to produce correct near-wall values for ν_T and either vanish or reach a limiting value inside the logarithmic overlap region. This is clearly
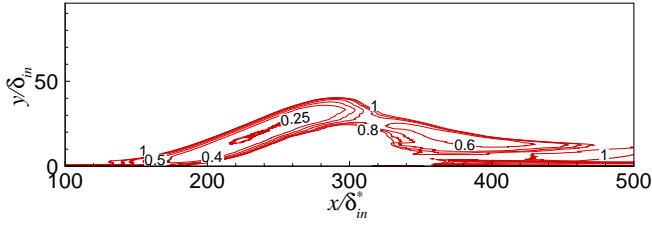
FIGURE 5. Contour lines of the exact value of f_μ calculated from equation (23)

not true for the regions near the separated bubble that causes erroneous prediction of the flow field in the separated bubble. However, there is no exact representation of this function that is derived from a particular modelling practice, and the modification of f_μ is not only required in the near-wall regions, but also in the outer shear layer in this case.

3.3 *A posteriori* **tests of the turbulence models**

Next, we consider the full application of the turbulence models to the flow under consideration. In Figure 6 we compare the results obtained with the Spalart-Allmaras and $k - \omega$ models. Excellent prediction of the separation point is obtained while the error in the calculation of reattachment point is comparable with the results obtained from the calculation with exact eddy-viscosity supplied from the LES results. Velocity profiles in the zero pressure gradient part of the domain and after reattachment are in good agreement with the LES results.

Profiles of the streamwise velocity and distribution of friction coefficient obtained form the $k - \varepsilon$ models are presented in Figure 7 which demonstrates that the wall treatment has a crucial role. The low-Reynolds-number model is incapable to predict separation for this test case in which the separation is caused by a strong adverse pressure gradient, while it predicts satisfactorily the flow over a backward-facing step [5]. However the prediction of the friction coefficient is highly improved when the two-layer wall treatment is applied. It should be noted that the improvement in velocity profiles in the separation region was only limited to a very close distance from the solid boundary.

In Figure 8 results obtained from the $\zeta - f$ model are presented. The model provides satisfactory results for the prediction of the separation point. The distribution of the fiction coefficient is also in a good agreement with the LES result. However, the reattachment point is not accurately captured.
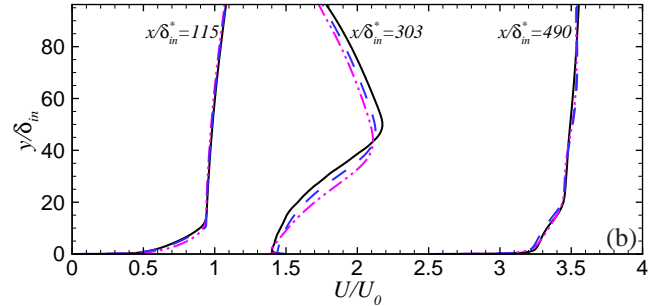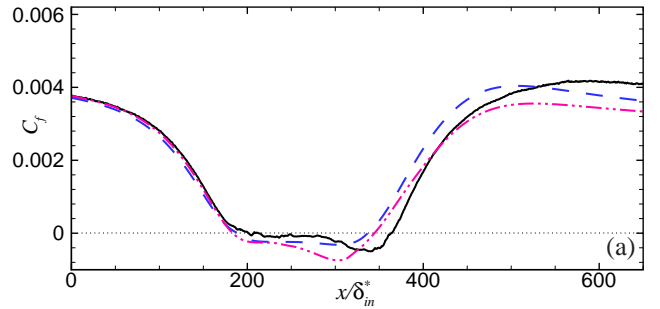
FIGURE 6. (a) Profiles of the friction coefficient and (b) streamwise velocity component. ——— LES; —··— Spalart-Allmaras model; – – – $k - \omega$ model.

4 Conclusion and recommendations for future work

This study investigated the performance of the most commonly used RANS models in the prediction of mild turbulent boundary layer separation. Some of the main issues of the eddy viscosity models have been addressed and examined in detail. The Boussinesq assumption was found to be valid in this flow despite the complex separated flow involved; note that anisotropic effects were not significant. The $k - \varepsilon$ model was found to be incapable to correctly predict non-equilibrium separated flows. Even the use of exact values of the turbulent kinetic energy and dissipation rate in the modeled eddy viscosity does not improve its performance. The damping function used in most low-Re number $k - \varepsilon$ models to improve the prediction of the near-wall turbulence was found to produce incorrect eddy viscosity in the region of the separated flows. The $k - \omega$, Spalart-Allmaras and $\zeta - f$ models, where the modification for the near-wall turbulence is not necessary, generally gives better results.

Future research is required to evaluate the model performance in other test cases which are in industrial interests. The relative performance of different models are to some extent uncertain due to the role of error cancellation involved in these models, *i.e.* the level of turbulent kinetic energy obtained from the $k - \omega$ model is highly underpredicted in the near-wall regions and use of the
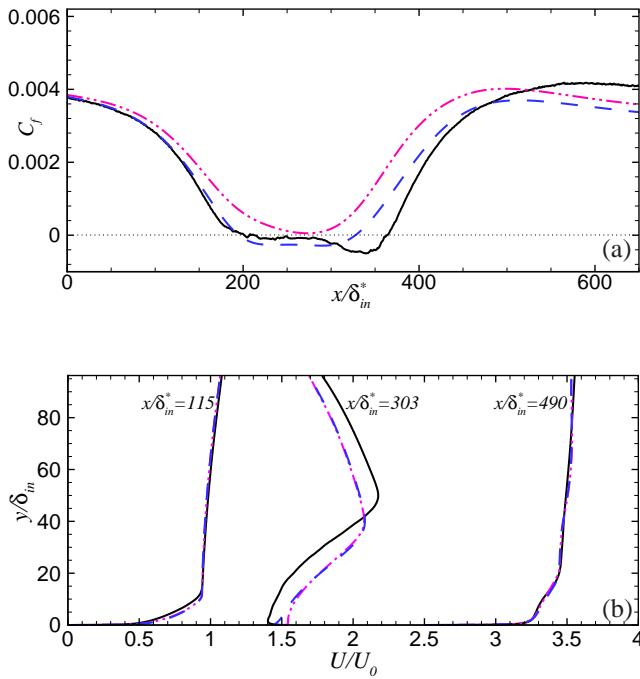
FIGURE 7. (a) Profiles of the friction coefficient and (b) streamwise velocity component. ——— LES; —··— Low-Re model; - - - RNG $k - \varepsilon$ model with two-layer wall treatment.
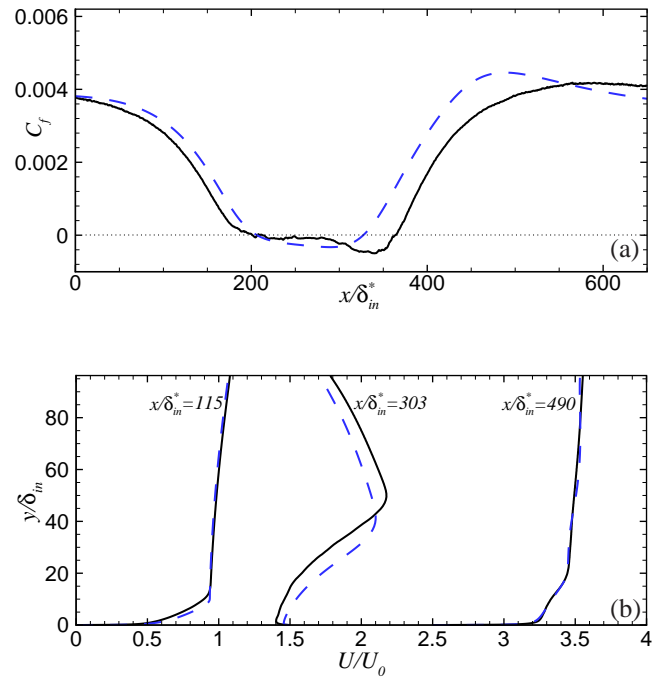
FIGURE 8. Distribution of friction coefficient (a), and streamwise velocity profiles (b): $\zeta - f$ model; ——— LES; - - - model prediction; —··— model prediction with exact k and ε

exact values of the LES results in the $k - \varepsilon$ model deteriorates its performance in the separated boundary layer. This posses a fundamental difficulty in drawing a conclusion on which model should be taken for general uses, or to isolate the causes of the failures.

REFERENCES

[1] Spalart, P. R., 2000, "Strategies for turbulence modelling and simulations," Int. J. Heat Fluid Flow, **21**, pp. 252–263.

[2] Apsley, D. and Leschziner, M., 2000, "Advanced Turbulence Modelling of Separated Flow in a Diffuser," Flow, Turbulence and Combustion, **63**(1), pp. 81–112.

[3] Wallin, S. and Johansson, A. V., 2000, "An explicit algebraic Reynolds stress model for incompressible and compressible turbulent flows," Journal of Fluid Mechanics, **403**(-1), pp. 89–132.

[4] V.C. Patel, W. R. and Scheuerer, G., 1985, "Turbulence models for near-wall and low-Reynolds-number flows: A review." AIAA, **23**, pp. 1308–1319.

[5] Sarkar, A. and So, R. M. C., 1997, "A critical evaluation of near-wall two-equation models against direct numerical simulation data," International Journal of Heat and Fluid Flow, **18**(2), pp. 197–208.

[6] Paneix, S. and Durbin, P., 1996, "A new methodology for turbulence modelers using DNS database analysis," Center for Turbulence Research, Annual Research Brief, pp. 17–30.

[7] Yang, Z. and Shih, T., 1993, "New time scale based - model for near-wall turbulence," AIAA, **31**.

[8] Yakhot, V., Orszag, S. A., Thangam, S., Gatski, T. B., and Speziale, C. G., 1992, "Development of turbulence models for shear flows by a double expansion technique," Phys. Fluids A, **4**(7), pp. 1510–1520.

[9] Yakhot, V. and Orszag, S. A., 1987, "Renormalization group and local order in strong turbulence," Nuclear Physics B - Proceedings Supplements, **2**, pp. 417–440.

[10] Wilcox, D., 1988, "Re-assessment of the scale-determining equation for advanced turbulence models," AIAA, **26**, pp. 1414–1421.

[11] Spalart, P. R. and Allmaras, S. R., 1994, "A One-Equation Turbulence Model for Aerodynamic Flows," La Recherche Aérospatiale, **1**, pp. 5–21.

[12] Hanjalic, K., Popovac, M., and Hadziabdic, M., 2004, "A robust near-wall elliptic-relaxation eddy-viscosity turbulence model for CFD," International Journal of Heat and Fluid Flow, **25**(6), pp. 1047–1051.

[13] Durbin, P. A., 1995, "Separated flow computations with the $k - \varepsilon - v^2$ model," AIAA Journal 1995, **33**, pp. 659–664.

[14] Meneveau, C., Lund, T. S., and Cabot, W. H., 1996, "A Lagrangian dynamic subgrid-scale model of turbulence," J. Fluid Mech., **319**, pp. 353–385.

[15] Keating, A., Piomelli, U., Bremhorst, K., and Nešić, S., 2004, "Large-eddy simulation of heat transfer downstream of a backward-facing step," J. Turbul., **5**(20), pp. 1–27.

[16] Demirdzic, I. A. and Peric, M., 1990, "Finite volume method for prediction of fluid flow in arbitrarily shaped domains with moving boundaries," International Journal for Numerical Methods in Fluids, **10-7**, pp. 771–790.

[17] Chen, H. and Patel, V., 1988, "Near-wall turbulence models for complex flows including separation," AIAA J., **26**, pp. 641–648.

[18] Speziale, C. and Thangam, S., 1992, "Analysis of an RNG based turbulence model for separated flows," International Journal of Engineering Science, **30**(10), pp. 1379–1388, IN3–IN4.

[19] Durbin, P. A., 1996, "On the $k - \varepsilon$ stagnation point anomaly," International Journal of Heat and Fluid Flow, **17**(1), pp. 89–90.

[20] Na, Y. and Moin, P., 1998, "Direct numerical simulation of a separated turbulent boundary layer," J. Fluid Mech., **370**, pp. 175–201.

[21] Lund, T. S., Wu, X., and Squires, K. D., 1998, "Generation of inflow data for spatially-developing boundary layer simulations," J. Comput. Phys., **140**, pp. 233–258.

[22] Durbin, P. A. and Petterson-Reif, B. A., 2001, *Statistical Theory and Modeling for Turbulent Flows.*, Wiley.